Journal of Power Sources 341 (2017) 327–339

Contents lists available at ScienceDirect

Journal of Power Sources

journal homepage: www.elsevier.com/locate/jpowsour

Electrochemical modelling of Li-ion battery pack with constant voltage cycling

T.R. Ashwin [a, b], A. McGordon [a], P.A. Jennings [a, *]

[a] WMG, University of Warwick, UK
[b] Centre for Scientific Computing, University of Warwick, Coventry, CV4 7AL, UK

HIGHLIGHTS

- P2D model is extended to a battery pack and demonstrated with four cells.
- The model integrates ageing, thermal and variable porosity prediction.
- Differential ageing of the cells and resulting current imbalance can be predicted.
- Thermal variations in the pack and thermally accelerated SEI growth is modelled.
- Differential porous filling can lead to current imbalance in the pack.

ARTICLE INFO

Article history:
Received 29 September 2016
Received in revised form
21 November 2016
Accepted 25 November 2016

Keywords:
Battery pack
Electro-chemical model
Ageing analysis
Variable porosity

ABSTRACT

In a battery pack, cell-to-cell chemical variation, or the variation in operating conditions, can possibly lead to current imbalance which can accelerate pack ageing. In this paper, the Pseudo-Two-Dimensional(P2D) porous electrode model is extended to a battery pack layout, to predict the overall behaviour and the cell-to-cell variation under constant voltage charging and discharging. The algorithm used in this model offers the flexibility in extending the layout to any number of cells in a pack, which can be of different capacities, chemical characteristics and physical dimensions. The coupled electro-thermal effects such as differential cell ageing, temperature variation, porosity change and their effects on the performance of the pack, can be predicted using this modelling algorithm. The pack charging voltage is found to have an impact on the performance as well as the SEI layer growth. Numerical studies are conducted by keeping the cells at different thermal conditions and the results show the necessity to increase the heat transfer coefficient to cool the pack, compared to single cell. The results show that the thermal imbalance has more impact than the change in inter-connecting resistance on the split current distribution, which accelerates the irreversible porous filling and ageing.

1. Introduction

The increasing popularity of portable devices and automobiles has accelerated research on energy storage devices, in particular lithium-ion batteries. The single cells can be easily assembled to a pack layout such as series, parallel or a combination of both, depending on the usage. Thus battery packs offer a clean, environmentally friendly option to store and deliver energy to meet the increasing demand; however it poses numerous problems, for example, each cell can be affected by the behaviour of its neighbour. The behaviour of a battery pack is found to be more technically challenging than a single cell since the neighbouring cell behaviour can affect each cell.

Single cell battery modelling has been the focus for much research and a substantial improvement has been made in predicting basic cell characteristics under various operating conditions [1,2]. The capacity fade of a battery can be predicted by introducing a continuous solvent reduction reaction [3,4]. Another important parameter is the operating temperature of the battery. Details of an accurate distributed thermal model can be found in Cai and White [5] and Ye et al. [6].

There are different methods of extending the single cell model to pack layout. Researchers use Equivalent Circuit Models (ECM) or

* Corresponding author.
E-mail addresses: A.T.Rajan@warwick.ac.uk (T.R. Ashwin), A.McGordon@warwick.ac.uk (A. McGordon), Paul.Jennings@warwick.ac.uk (P.A. Jennings).

http://dx.doi.org/10.1016/j.jpowsour.2016.11.092

Electro-Chemical based Models (EChM) to simulate a pack behaviour from a single cell. Again, the modelling approach is divided into two categories. The first approach in battery pack modelling is to build a single battery pack model for the entire circuit therefore neglecting the internal current distribution under the assumption of homogeneity. A pack modelling approach based on this method assumes that all cells are perfectly balanced and uniformly cooled so that an isotropic assumption can be applied to all cells which may not be the case in reality. Important examples can be found in Dubarry et al. [7] and Kim et al. [8]. All the above reported experiments and modelling were heavily dominated by the assumption of homogeneity which neglects the real world variation.

The second widely accepted method, and also used in this paper, is to solve each cell independently and integrate the cell responses for a particular layout. This modelling approach offers a high degree of fidelity and flexibility in choosing the layout. Moreover the model can easily capture cell-to-cell variation in a pack imposed due to the build-up of internal resistances and property variations. The widely accepted method is to assemble ECM based models due to their simplicity and faster computing power. A Battery Management System (BMS) perspective of this modelling approach can be seen in Sen and Kar [9] and Kroeze and Krein [10]. However the ECM based models do not inherently represent the capacity fade and thermal variation as a result of chemical (side) reactions; this can be included based on experimental data-driven results.

The electro-chemical extension of the single cell model to a pack layout is considered to be highly accurate because these models can capture the complex non-linear chemical reactions inside the anode and cathode and therefore accurately calculate the ageing and temperature variation inside a battery pack. High computing power requirement was one of the main reasons preventing researchers from using electro-chemical-based pack models. However in recent years there have been significant improvements in computing resources and the computational methods, especially in reduced order models [11,12] which can be possibly extended to a battery pack model.

The simplest electro-chemical model is the Single Particle model (SP) which has only a single particle in the anode and cathode. The work by Kenney et al. [13] extended the SP electrochemical model for a pack of batteries connected in series. Though this model was the first attempt in extending the EChM model for a battery pack, the numerical accuracy was questioned due to the single particle approximation [14]. Important thermal models for a battery pack can be found in Sun et al. [15], Severino et al. [16], and Mills and Hallaj [17]. However these models are either without the important factors such as ageing and porosity variation, or the cells are considered as a heat generating object without any electro-chemistry. The Pseudo Two Dimensional (P2D) model is an extension of the SP model over a rigorous porous layout. P2D model assumes that the electrodes are filled with homogeneous solid particles of uniform dimension. The solid concentration is solved over the radial coordinates at a particular cartesian location over time, giving a pseudo two dimensional dependency for the model; thus the name Pseudo Two Dimensional Model. One of the more significant and recent work is by Wu et al. [18] who extended the P2D model for a battery pack with interconnected resistance with a lumped thermal model, however the impact of differential cell heating and internal resistance on the capacity fading was not modelled.

From the literature, and also to the best of author's knowledge, there are no investigations on extending a rigorous P2D model for a pack layout, with any of coupled ageing, distributed thermal and porosity variation. The model described here achieves all three of the above. Though not addressed in this paper; the porous filling can be correlated to the possible stress development in the cells in a battery pack leading to the expansion of cells in use [19]. Unlike the single cell operation, cell-to-cell variation always exists in a pack due to manufacturing differences. Operating conditions can also change the internal resistance of the individual cells in the pack. The manufacturing variation and the Solid Electrolyte Interphase (SEI) growth can cause an imbalance in the cell-to-cell split current, depending on the pack layout. Thus, an ideal pack model should be capable of accounting for the manufacturing variations and operating conditions. This can also cause differential thermal heating which can accelerate the differential porous filling and possibly lead to differential internal stress development and hence differential cell behaviour. A distributed thermal model is needed to analyse thermal variations precisely. Coupling of the electro-chemical-thermal model with an ageing model is found to be important in capturing the impact of operating conditions on pack life [20]. The present paper proposes a solution for all the above mentioned problems and incorporates the required capabilities under a strong and fast numerical scheme.

A P2D model combining ageing, distributed thermal and variable porosity and solved using an implicit scheme is presented in Ashwin et al. [21]. The work presented in this paper is an extension of the single cell finite volume based model developed for $LiCoO_2$ chemistry. The electrochemical parameters for this model are taken from Smith and Wang [2], ageing parameters from Ramadass et al. [3], thermal model from Cai and White [5] and the variable porosity from Sikha [22]. A general pack configuration and the cell balancing equations have been adapted from Wu et al. [18] to calculate the current flow to each individual cell by solving Kirchhoff's law.

The model integrates for the first time; the capacity fading solvent reduction reaction, thermal heat generation and the porosity change due to intercalation reaction for a pack layout with a constant voltage charging configuration. The pack is cycled between two voltage limits, upper pack voltage and lower pack voltage, with a constant voltage input. Unlike constant current charging, the constant voltage charging results in a time varying current profile. The modelling is done with diverse operating conditions and conclusions are made on the individual cell characteristics including the ageing and thermal signature of each cell in the pack.

A novel approach has been adopted for modelling the cell resistance, which is a key parameter in deciding the split current distribution, where the total cell resistance has a contribution from the internal resistance and also the internal resistance due to the SEI. The internal resistance of the cell is taken as a function of State of Charge (SoC) and temperature. Kirchoff's current and voltage balance is modified to include the additional internal resistance due to SEI growth. The formulation adopted in this paper can be extended to any number of cells in the same layout, making it easier to analyse a bigger pack. The chemical variables in this model are temperature corrected using an Arrhenius equation. The convective heat transfer coefficient can be set to different values to replicate different thermal operating conditions with forced convection and natural convection. The model is also able to investigate the effect of irreversible porous filling due to the solvent reduction side reaction.

The paper is structured as follows: Section 2 presents the battery pack layout. Governing equations for the pack layout are listed in Section 3 while the solution methodology and the algorithm is listed in Section 4. Modelling results are presented in Section 5, followed by a detailed discussion in Section 6 and conclusion in Section 7.

2. Battery pack layout

Fig. 1 presents the pack configuration with four cells connected

neither series nor parallel. This layout is adapted from Wu et al. [18] and reformulated for a 4 cell pack configuration with Li_yCoO_2 chemistry. The particular configuration is selected to distribute the charging and discharging voltage equally in all branches which in-turn can control the split current. This same modelling layout can be extended to any number of cells, however the cell number is limited to four for simplicity in this manuscript. This layout is with equal inter-connecting resistance but it can be varied depending on the usage with minor modification in the Kirchoff's current balance. With zero inter-connecting resistance, the pack reduces to a parallel configuration with equal distribution of split current. The safe upper cut off voltage and lower cut off voltage of the individual cells assembled in this pack is chosen as 3.89 V and 3.32 V respectively [2]. The charging and discharging voltage of the pack is different from the individual cell voltages. Thus the Pack Charging Voltage (PCV) and the Pack Discharging Voltage (PDV) are kept at 4.2 V and 3.3 V to completely charge or discharge individual batteries. The applied pack voltage is changed from PCV to PDV, once any of the individual cells reaches the cell cut-off limit, i.e. 3.89 V. Similarly, the cut off voltage will be reversed from PDV to PCV if any one of the cells in the pack reaches the lower cut-off limit of that cell, i.e. 3.32 V. The pack is thus cycled between the voltage limits depending on the individual cells reaching the cut off limits. Section 5.1 in this work describes a sensitivity study conducted to study the variation of charging current with pack upper cut off voltage. The voltage difference between the cells and the pack is necessary to push energy into and out of the cell. Results show that keeping the pack charging voltage equal to the upper limit of Open Circuit Voltage (OCV) of the cell can result in infinite time for charging. Similarly keeping the pack discharge voltage equal to the lower limit of OCV can result in infinite time for discharging. Thus the threshold voltage selection is critical in charging or discharging of individual cells connected in the pack.

3. Governing equations

The governing equations for a Newman model are already listed in the previous publication by Ashwin et al. [21]. The capacity fading and variable porosity can be included as follows:

The solvent reduction reaction is given by:

$$J_s = -a_n i_{os} e^{\left(\frac{-a_c F \eta_s}{RT}\right)} \tag{1}$$

The rate of SEI layer increase over a particular cycle is proportional to the solvent reduction reaction current density.

$$\frac{\partial}{\partial t}\delta_{film} = -\frac{J_s M_{SEI}}{a_n \rho_{SEI} F} \tag{2}$$

The battery is assumed to start with the initial Ω_{SEI} resistance. Thus, Ω_{SEI} is considered only in the first cycle. The total resistance of the SEI layer is calculated by dividing the thickness of SEI layer with conductivity [3].

The SEI layer resistance can be calculated as:

$$G_{film}|_N = \Omega_{SEI}|_{N=0} + \frac{\delta_{film}|_N}{\kappa_{SEI}} \tag{3}$$

For each cycle the thickness and resistance keep increasing over time according to

$$\delta_{film}|_N = \delta_{film}|_{N-1} + \delta_{film}(t) \tag{4}$$

The porosity variation can be taken proportional to the partial molar concentration of the electrolyte [22].

$$\frac{\partial \varepsilon_e}{\partial t} = a_{n,p}(J_1\, V_{Li^+} + J_s\, V_{Lac}) \tag{5}$$

The interfacial surface area is given by Refs. [2,5].

$$a_{n,p} = 3\varepsilon_{s(n,p)} \Big/ \Lambda_{s(n,p)} \tag{6}$$

The energy balance for the battery heat generation is given by:

$$\rho C_p \frac{\partial T}{\partial t} = \lambda \frac{\partial^2 T}{\partial x^2} + Q_{react} + Q_{rev} + Q_{ohm} \tag{7}$$

where Q_{react} is the heat generation due to reaction inside the battery, Q_{rev} is the reversible heat generation and Q_{ohm} is the Ohmic heat generation rate. Each term in the above equation is defined as follows:

$$Q_{\text{react}} = J(\phi_s - \phi_e - U),$$

$$Q_{\text{rev}} = TJ\frac{\partial U}{\partial T},$$

$$Q_{\text{ohm}} = \sigma_{eff}\left(\frac{\partial \phi_s}{\partial x}\right) + \kappa_{eff}\left(\frac{\partial \phi_e}{\partial x}\right)^2 + \frac{2\kappa_{eff}RT}{F}\left(1 - t_+^0\right)\frac{\partial \ln c_e}{\partial x}\quad\frac{\partial \phi_e}{\partial x}.$$

The total heat generated inside the battery is convected to the ambient by the Newton law of cooling.

$$-\lambda\frac{\partial T}{\partial x}|_{x=0} = h(T_{\text{amb}} - T)\ and\ -\lambda\frac{\partial T}{\partial x}|_{x=L} = h(T - T_{\text{amb}})$$

The applied external voltage remains the same for all closed loops (Ref. Fig. 1) considered in this pack. Kirchhoff's voltage balance equation can be applied to the closed loop to relate the individual cell voltage to the pack voltage (PCV or PDV). Within the

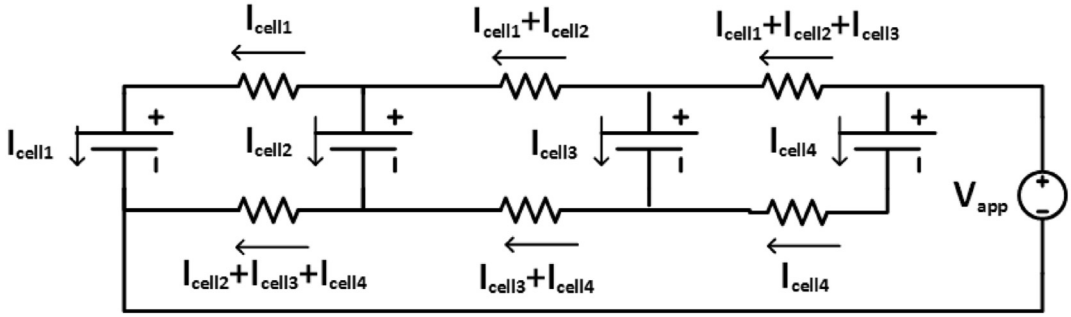

Fig. 1. Battery pack layout with constant voltage charging and discharging. Cells connected with inter-connecting resistance R_c.

closed loop, the voltage is summed to zero and four such loops can be identified in this pack. At steady state, the individual cell voltage can be related to the pack applied voltage and closed loop will give four different equations which govern the current flow through the system.

$$V_{app} = OCV_{cell1} + \eta_{cell1} + R_c(3I_{cell1} + 2I_{cell2} + I_{cell3} + 0I_{cell4}) \quad (8)$$

$$V_{app} = OCV_{cell2} + \eta_{cell2} + R_c(2I_{cell1} + 3I_{cell2} + 2I_{cell3} + I_{cell4}) \quad (9)$$

$$V_{app} = OCV_{cell3} + \eta_{cell3} + R_c(I_{cell1} + 2I_{cell2} + 3I_{cell3} + 2I_{cell4}) \quad (10)$$

$$V_{app} = OCV_{cell4} + \eta_{cell4} + R_c(0I_{cell1} + I_{cell2} + 2I_{cell3} + 3I_{cell4}) \quad (11)$$

The above system of equations for 4 cells can be extended to a circuit with N number of cells as follows

$$\begin{bmatrix} V_{app} \\ \vdots \\ V_{app} \end{bmatrix} = \begin{bmatrix} OCV_{cell_1} + \eta_{cell1} \\ \vdots \\ OCV_{cell_N} + \eta_{cellN} \end{bmatrix} + \begin{bmatrix} N-1-|i-j| & \cdots & N-1-|i-N| \\ \vdots & \ddots & \vdots \\ N-1-|N-j| & \cdots & N-1-|N-N| \end{bmatrix} \begin{bmatrix} I_{cell1} \\ \vdots \\ I_{cell_N} \end{bmatrix} R_c \quad (12)$$

Where i and j are the row and column number of the matrix with $N \times N$ cells.

The over potential of the battery is the product of the split current of the cell and the overall cell resistance. In this formulation, the cell resistance is divided into two components, the resistance increase of the cell due to the solvent reduction side reaction (SEI formation) and the contribution from cell internal resistance which is taken as a function of SoC and operating temperature. Applying the above approximation to the system of equations:

$$\begin{bmatrix} OCV_{cell_1} + I_{cell_1}(R_{SEI_1} + R_{cell_1}) \\ \vdots \\ OCV_{cell_N} + I_{cell_N}(R_{SEI_N} + R_{cell_N}) \end{bmatrix} + \begin{bmatrix} N-1-|i-j| & \cdots & N-1-|i-N| \\ \vdots & \ddots & \vdots \\ N-1-|N-j| & \cdots & N-1-|N-N| \end{bmatrix} \begin{bmatrix} I_{cell1} \\ \vdots \\ I_{cell_N} \end{bmatrix} R_c = \begin{bmatrix} V_{app} \\ \vdots \\ V_{app} \end{bmatrix} \quad (13)$$

The internal resistance of each cell is averaged and taken as the resistance of the pack at a particular time step. Thus over a time step, the resistance of a cell R_{cell} can be approximated to a constant value. The resistance of each cell due to build-up of SEI layer thickness is calculated from Equation (3).

$$R_{cell} \begin{bmatrix} I_{cell1} \\ \vdots \\ I_{cell_N} \end{bmatrix} + \begin{bmatrix} I_{cell1}R_{SEI_1} \\ \vdots \\ I_{cellN}R_{SEI_N} \end{bmatrix} + \begin{bmatrix} N-1-|i-j| & \cdots & N-1-|i-N| \\ \vdots & \ddots & \vdots \\ N-1-|N-j| & \cdots & N-1-|N-N| \end{bmatrix} \begin{bmatrix} I_{cell_1} \\ \vdots \\ I_{cell_N} \end{bmatrix} R_c = \begin{bmatrix} V_{app} - OCV_{cell_1} \\ \vdots \\ V_{app} - OCV_{cell_N} \end{bmatrix} \quad (14)$$

Rearranging the contribution from SEI layer:

$$R_{cell} \begin{bmatrix} I_{cell1} \\ \vdots \\ I_{cell_N} \end{bmatrix} + \begin{bmatrix} N-1-|i-j| & \cdots & N-1-|i-N| \\ \vdots & \ddots & \vdots \\ N-1-|N-j| & \cdots & N-1-|N-N| \end{bmatrix} \begin{bmatrix} I_{cell1} \\ \vdots \\ I_{cell_N} \end{bmatrix} R_c + \begin{bmatrix} I_{cell_1} \\ \vdots \\ I_{cell_N} \end{bmatrix} R_c = \begin{bmatrix} V_{app} - OCV_{cell_1} - I_{cell1}R_{SEI_1} \\ \vdots \\ V_{app} - OCV_{cell_N} - I_{cellN}R_{SEI_N} \end{bmatrix} \quad (15)$$

Rearranging the system of equations:

$$\begin{bmatrix} I_{cell1} \\ \vdots \\ I_{cell_N} \end{bmatrix} \begin{bmatrix} (N-1-|i-j|)\frac{R_c}{R_{cell}} + 1 & \cdots & (N-1-|i-N|) \\ \vdots & \ddots & \vdots \\ (N-1-|N-j|) & \cdots & (N-1-|N-N|)\frac{R_c}{R_{cell}} + 1 \end{bmatrix} = \frac{1}{R_{cell}} \begin{bmatrix} V_{app} - OCV_{cell_1} - I_{cell1}R_{SEI_1} \\ \vdots \\ V_{app} - OCV_{cell_N} - I_{cellN}R_{SEI_N} \end{bmatrix} \quad (16)$$

Thus the governing equations can be concised into the matrix form [X] = [B] $[A]^{-1}$ where A is the operator matrix, X is the current vector and B is the applied voltage matrix.

$$\begin{bmatrix} I_{cell1} \\ \vdots \\ I_{cell_N} \end{bmatrix} = \frac{1}{R_{cell}} \begin{bmatrix} V_{app} - OCV_{cell_1} - I_{cell1}R_{SEI_1} \\ \vdots \\ V_{app} - OCV_{cell_N} - I_{cellN}R_{SEI_N} \end{bmatrix} \begin{bmatrix} \beta_{1,1} & \cdots & \beta_{1,N} \\ \vdots & \ddots & \vdots \\ \beta_{N,1} & \cdots & \beta_{N,N} \end{bmatrix} \quad (17)$$

Table 1
Electro-chemical modelling parameters of 6 Ah single cell assembled in the pack.

	Negative electrode	Separator	Positive electrode
Parameters for base battery model			
Thickness, δ (cm)	50×10^{-4}	25.4×10^{-4}	36.4×10^{-4}
Particle radius, Λ_s (cm)	1×10^{-4}		1×10^{-4}
Active material volume fraction ϵ_s	0.580		0.500
Electrolyte phase volume fraction ϵ_e	0.332	0.5	0.330
Maximum solid phase concentration $c_{s,max}$ (mol cm^{-3})	16.1×10^{-3}		23.9×10^{-3}
Stoichiometry at 0% SOC	0.126		0.936
Stoichiometry at 100% SOC	0.676		0.442
Average electrolyte concentration c_e (mol cm^{-3})	1.2×10^{-3}	1.2×10^{-3}	1.2×10^{-3}
Exchange current density (i_o) (A cm^{-3})	3.6×10^{-3}		2.6×10^{-3}
Charge-transfer coefficients α_a, α_c	0.5, 0.5		0.5, 0.5
SEI layer film resistance, Ω_{SEI} (Ω cm^2)[a]	100		100
Solid phase Li diffusion coefficient, D_s (cm^2 s^{-1})	2.0×10^{-12}		3.7×10^{-12}
Solid phase conductivity, σ (S cm^{-1})	1.0		0.1
Electrolyte phase Li^+ diffusion coefficient, D_e (cm^2 s^{-1})	2.6×10^{-6}	2.6×10^{-6}	2.6×10^{-6}
Bruggeman porosity exponent, p	1.5	1.5	1.5
Electrolyte activity coefficient, $f^{\pm}$	1.0	1.0	1.0
Li^+ transference number, t_+^0	0.363	0.363	0.363
Parameters for solvent reduction side reaction			
Reference voltage U_{ref} (V)[a]	0		0
Molecular weight M_{SEI} (kg mol^{-1})	7.3×10^4		
Density of SEI Layer ρ_{SEI} (kg cm^{-3})	2.1×10^{-3}		
Side reaction exchange current density i_{os} (A cm^{-3})[a]	1.5×10^{-12}		
Conductivity of SEI Layer κ_{SEI} (S cm^{-1})[a]	1×10^{-4}		
Parameters for thermal model			
Density of electrolyte ρ_e (kg cm^{-3})	1123.0×10^6	1123.0×10^6	1123.0×10^6
Density of solid phase ρ_s (kg cm^{-3})	1347.3×10^6		2328.5×10^6
Electrolyte thermal Conductivity λ_e (W cm^{-1} K^{-1})	3.39×10^{-2}	3.39×10^{-2}	3.39×10^{-2}
Solid phase thermal conductivity λ_s (W cm^{-1} K^{-1})	3.39×10^{-2}		3.39×10^{-2}
Heat capacity of solid C_p (J kg^{-1} K^{-1})	1437.4	1978.2	1669.2
Electrolyte heat capacity C_p (J kg^{-1} K^{-1})		2055.1	
Parameters for variable porosity			
Partial molar volume for main reaction V_{Li^+} (cm^3 mol^{-1})	5.0		
Partial molar volume for side reaction V_{Lac} (cm^3 mol^{-1})	64.39		

[a] Values from Ashwin et al. (2016), [21].

4. Algorithm flow chart

The governing equations for electrolyte concentration, solid potential and electrolyte potential are solved at the nodal point corresponding to the centre of the control volume; the solid concentration is solved at radial nodes at each cartesian nodal point. The equations are solved in sequence, coupled with Butler-Volmer kinetics. The equations are iterated in a coupled way until the residual error reduces below a threshold value. Details of the finite volume method can be seen in Patankar [23] and its application in Ashwin et al. [24]. An in-house Fortran program was developed to solve the coupled governing equations using a finite volume method. The program has been validated against the publications of Smith and Wang [2], Ramadass et al. [3] and Cai and White [5]; more details of the validation study can be found in Ashwin et al. [21]. The individual cell behaviour is again validated with a similar pack layout proposed by Wu et al. [18] to ensure the accuracy of the prediction. The split current variation is following the trend while the thermal behaviour cannot be compared directly since Wu et al. [18] was using a lumped thermal model whereas the present model uses a discrete thermal model for better accuracy. The properties of the battery used are listed in Table 1. The same formulation is adopted in this pack layout using the algorithm presented in Fig. 2.

The cell initialisation subroutine defines the grid generation and initialises the chemical parameters of each individual cell in the pack. The difference in cell chemistry, solvent reduction side reaction parameters and the initial SEI thickness can be included in this subroutine. Many of the practical issues, for example prelithiation can be captured by increasing the initial solid concentration. Differentially aged cells can be modelled by setting different initial SEI resistances which increases the internal resistance of the relevant cells in the pack. The grid generation subroutine has the flexibility to vary the size and capacity of each cell. Also this grid layout allows the mesh density to be varied at locations where the gradient of chemical change is large allowing a non-uniform mesh. The current distribution to each cell at a particular time step is calculated by solving Kirchoff's network law for the circuit shown in Fig. 1. The governing equations applied to the closed loop are solved to calculate the split current to each cell in the pack. Fortran in-built matrices operation can be used to invert and solve the system of matrix. The split current for each cell is calculated at the beginning of each time step and used as the charging or discharging current for each cell at a particular time step. Each individual cell in the battery is started with 0% SoC condition and the pack is cycled according to the guidelines presented in the previous section. The cut off condition ensures the safe operation of the individual cells by reversing the voltage if any one of the cell reaches the cut off limit thereby avoiding overcharge or over discharge. The running time of the model is monitored, or the flux imbalance is checked, for the exit condition. An accuracy of 0.001 V (A) for both current and voltage is enough to give accurate results for the calculations presented in this work.

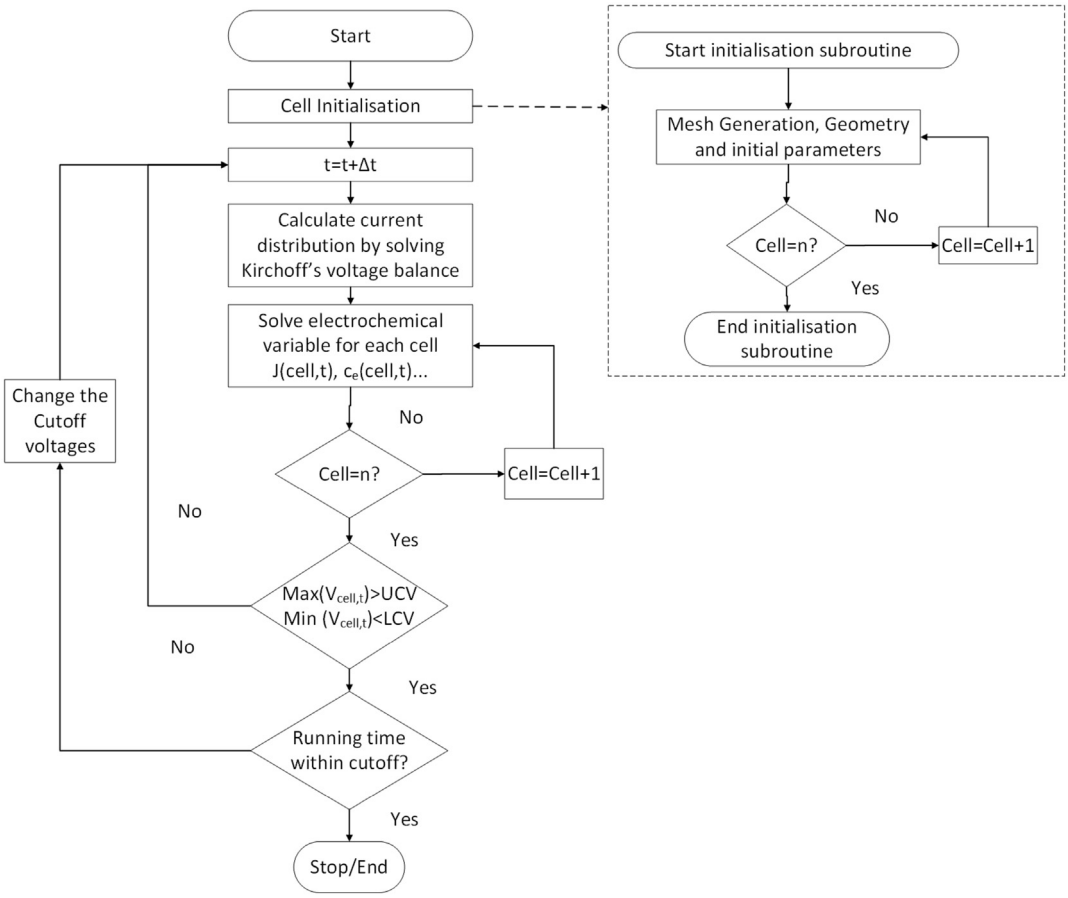

Fig. 2. Flow chart for the algorithm used in multi-cell calculation.

5. Results

The results are broadly divided into four sections which discuss the battery pack performance under different operating conditions. Proper care has been given to include diverse operating conditions and to analyse the effect on the battery performance. Though most of the results are coupled and interlinked; the impact of different chemical and operating conditions are studied by turning off or turning on the corresponding governing equations. Section 5.1 discusses the variation of current and voltage in individual cells with the change of pack charging voltage. Section 5.2 discusses the porosity variation on the battery performance. Section 5.3 analyses the SEI growth on individual cells in the pack and the impact on overall pack performance. Section 5.4 shows the thermal influence on the performance of the battery and the results are presented for a battery pack operating at an elevated temperature. The temperature variations are simulated based on the practical situations which may be encountered during operation of any pack.

5.1. Voltage and current distribution in the pack

The current distribution to the individual cells in the pack can be altered by changing the inter-connecting resistance (R_c) connected to the circuit. Setting R_c to zero results in a parallel combination of cells connected to a voltage source or sink thereby equally distributing the charging and discharging current in all branches. Similarly, a non zero R_c can cause unequal current distribution to individual cells. A parallel configuration results in equal SEI growth and thermal characteristics as long as the chemical configuration of the cells is identical. Thus Fig. 3 presents results for a parallel identical pack layout and $Cell_1$ is taken as the sampling cell to plot the results.

Fig. 3a shows the current distribution for the first few charging and discharging cycles with different PCV. The charging and discharging procedure used in this paper is Constant Voltage (CV) charging and discharging by changing the V_{app} to PCV or PDV if any one of the cell in the pack reaches individual cut off limit. As already mentioned, the individual cell cut off limits are 3.89 V and 3.32 V at 100% and 0% SoC respectively [2]. The individual cell discharge profiles remain unaffected by the change in PCV whereas the charging profile changes. Charging the pack with 4.1 V PCV takes more than one hour while charging with 4.5 V PCV takes less than 30 min. The controlling parameter is the difference in pack charging voltage and the OCV of the individual cells. In this case, the OCVs are equal since the cells have same chemistry and are started with the same SoC. The pack charging voltage should be decided based on the upper limit of OCV (at 100% SoC) of the individual cells connected in the pack. At the limit where the PCV equals the upper limit of OCV, the cell takes infinite time for charging. This is otherwise represented in battery pack Equation (17) where $\left[I_{app}\right]_{1\times N} \propto \left[V_{app} - OCV\right]_{1\times N}$.

Similarly Fig. 3b shows the current distribution to the individual cells for the first charging and discharging cycle with different PDV. The charging profile remains unaffected in this case whereas the discharge profile changes shape. The limiting factor in this case is the lower limit of OCV and the PDV. The cell takes infinite time for discharging if the PDV and the lower limit of OCV (at 0% SoC) are equal. Thus the pack must be charged and discharged at a voltage

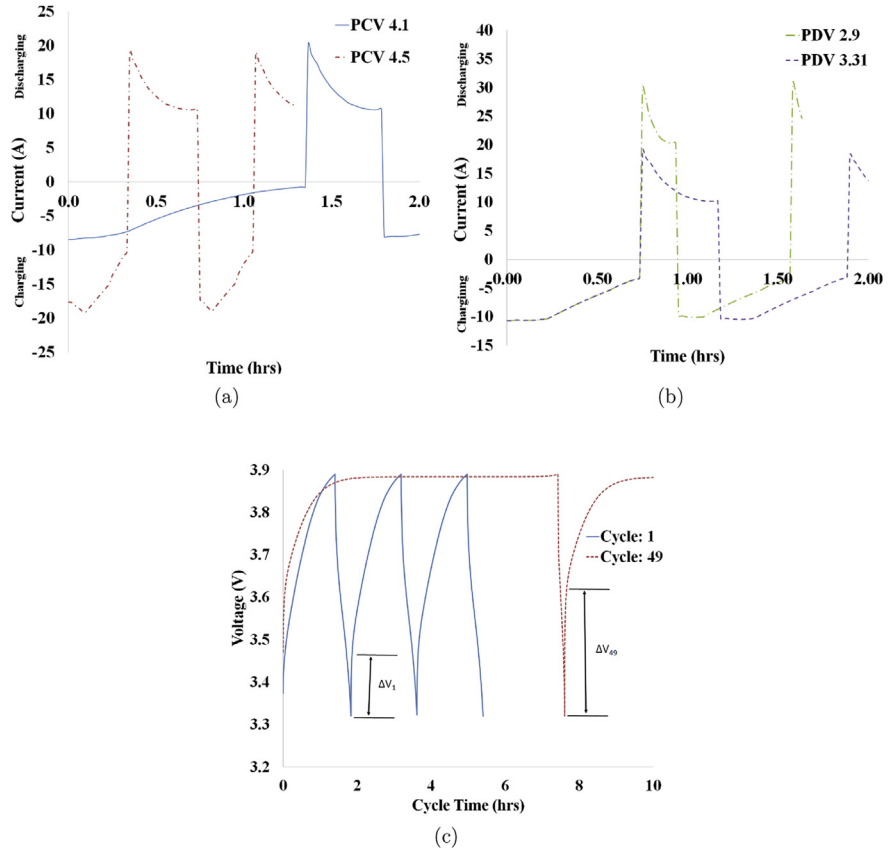

Fig. 3. Constant voltage charging profiles in $Cell_1$ with $R_c = 0$ (a) Current profile in $Cell_1$ with pack charging voltage, 4.1 V and 4.5 V (b) Current profile in $Cell_1$ with pack discharge voltage, 3.31 V and 2.9 V (c) Voltage profile after 50 Cycles of operation.

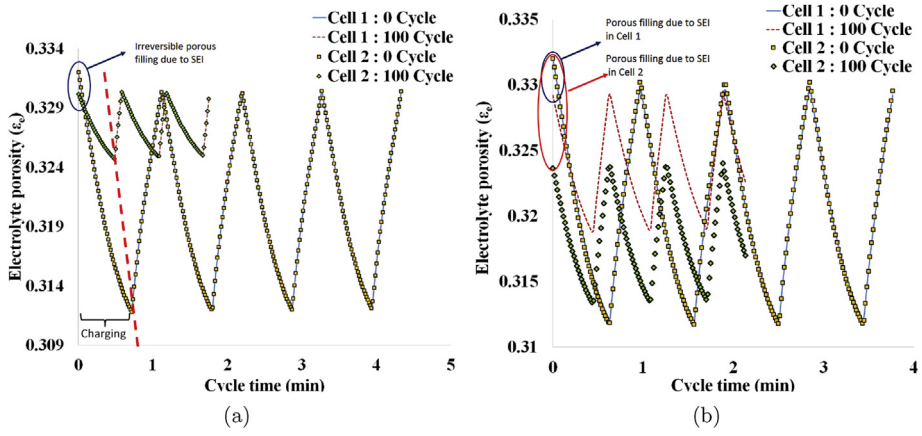

Fig. 4. Porosity variation in different cells in the pack, indicating irreversible filling due to SEI under constant voltage charging (a) Porosity change when all cells kept at identical chemical and thermal condition (b) Porosity for cells at different temperature with all other conditions identical.

above and below the OCV limit of the individual cells to charge and discharge the individual cells fully.

Fig. 3c shows the voltage profile variation after 50 constant voltage charging and discharge cycling with 4.1 V PCV and 3.31 V PDV. A solvent reduction side reaction dampens the overall current density, reducing the rate of chemical reaction which will be reflected in the model as the reduction in capacity. The time for charging increases to 8 h as the SEI layer thickens, indicating that the external power source has to overcome the resistance due to SEI, to charge the battery. A clear voltage jump can be seen at the beginning of the charge and discharge profile (after 50^{th} cycle) once the SEI layer develops. Thus, care should be taken to avoid the operating condition where the voltage drop by the SEI layer can affect the pack charging time. A voltage increase is suggested; otherwise this could lead to extremely long time for charging and very short time for discharging due to the dominance of SEI resistance. Thus, the pack charging voltage is taken as 4.2 V and the discharge voltage is 2.9 V which is sufficient to overcome the resistance offered by the SEI layer for the parameters considered in this study. The 4.2 V is determined by conducting a parametric

study by varying PCV from 3.89 V to 4.5 V such that the pack will be able to be charged within one hour even after 50 cycles of SEI growth. The 2.9 V value is determined in a similar way to discharge the battery within one hour after 50 cycles of SEI growth. The authors found that the PCV with 4.1 V is reaching flat asymptotic voltage profile after 20 cycles of SEI build up. This indicates that a PCV adjustment is needed as the pack gets older.

5.2. Effect of porosity variation on the pack performance

Fig. 4 shows the effect of variable porosity on the performance of the battery. The variable porosity has an impact on the volume specific area available for reaction. The area change is governed through the equation $a_s = 3\varepsilon_s/\Lambda_s$. The intercalation current density in the negative electrode is taken as negative during charging in this model. The current density changes sign during discharge and in the positive electrode. The amount of porous filling is controlled by the partial molar concentration of the electrolyte V_{Li^+} and V_{Lac}. The V_{Li^+} of the electrolyte corresponds to the reversible porosity variation whereas V_{Lac} represents the irreversible deposition over the particle due to SEI formation. The ageing reaction will get activated only during the charging process and is completely absent during discharge. This gradually increases the solid volume fraction of the battery during charge-discharge cycling. The value of the molar concentration should be adjusted to match the experimental results. However, no attempt has been made in this study to match the value with actual experimental results since this work is initially a theoretical model demonstration.

Fig. 4a shows that with zero inter-connecting resistance, the porosity in $Cell_1$ and $Cell_2$ is equal after a hundred cycles. This result indicates that the split current distribution is uniform without any imbalance, if operated with identical thermal and chemical conditions. A dashed line is used in the figure to separate charging region and the discharging region for the initial cycle for both the 0 and 100 cycle. The overall cycle time decreases over time due to the build-up of SEI layer which has developed uniformly in all the cells after a hundred cycles. Another interesting observation is the range of reversible porosity change, which is maximum for a fresh cell where the porosity changes from 0.334 to 0.310. The reversible porosity change decrease from 0.329 to 0.324 after a hundred cycles which indicates that the intercalation current density is substantially reduced or overpowered due to the build-up of SEI layer. The decrease in electrolyte porosity ε_e (or the increase in solid porosity ε_s) after a hundred cycles is caused by the irreversible filling of pores due to SEI growth.

Other imbalances such as thermal or unequal current distribution can alter this equilibrium and such a condition is presented in Fig. 4b where $Cell_2$ is kept at a higher temperature compared to $Cell_1$. The results show that the porous filling in $Cell_2$ gets accelerated compared to $Cell_1$ which is kept at a lower temperature. The higher temperature accelerates the solvent reduction reaction current density thereby causing an increased SEI layer growth. Thus the irreversible porosity change due to side reaction gets accelerated by the change in temperature. Later in this work, the results show that temperature is more crucial than controlling the split current by changing R_c.

5.3. Effect of capacity fade and SEI growth on the performance with non zero R_c

A non-zero inter-connecting resistance (R_c) can cause imbalance in the pack current, changing the magnitude of split current to individual cells. Fig. 5 shows the current distribution in the pack and the corresponding SEI growth. A non-zero resistance will result

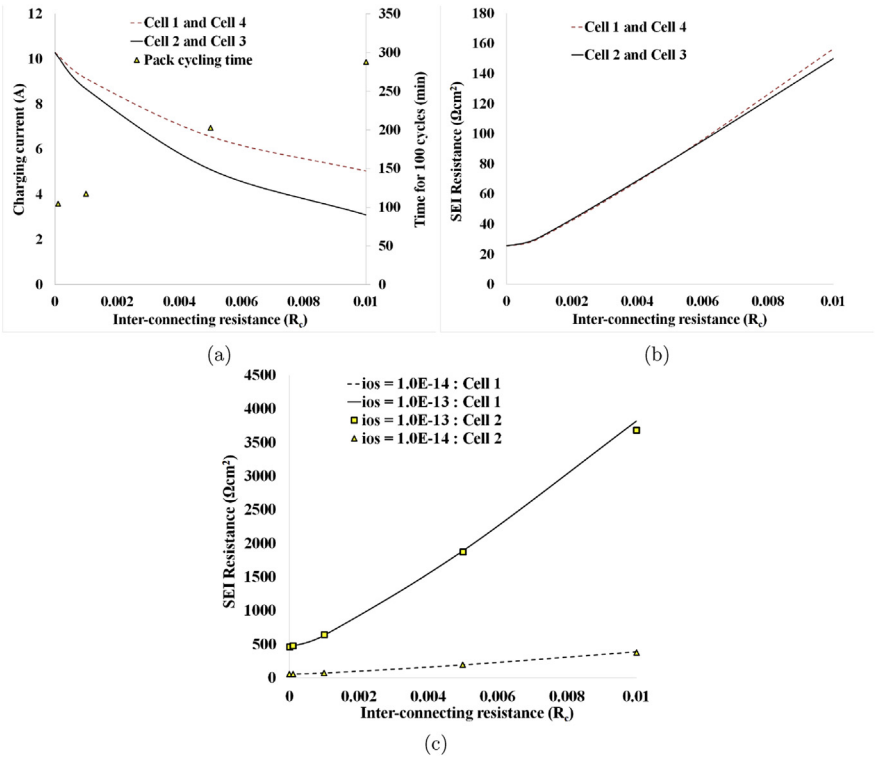

Fig. 5. Individual cells response in the pack with non-zero inter-connecting resistance R_c (a) Charging (split) current distribution after 100 cycles (b) SEI resistance after 100 cycles with $i_{os} = 1.5 \times 10^{-15}$ A cm^{-3} (c) SEI with different i_{os}.

in driving less current with equal magnitude in $Cell_2$ and $Cell_3$ and higher magnitude equal current in $Cell_1$ and $Cell_4$. This current imbalance can be seen in a pack with any number of cells, and here the outermost cells receive more current compared to the inner ones. The imbalance can be changed by using different R_c values for different branches. However, this model assumes that all inter-connecting resistances are equal, though this model is capable of including unequal resistance with a slight change in the Kirchoff's formulation.

Fig. 5a shows the current distribution at the beginning of a charging cycle after a hundred cycles of operation. An increase in the inter-connecting resistance decreases the cell charging current where the highest charging current is observed where the cells are connected in parallel without the resistance. Similarly the cells take a longer time to complete a hundred cycle with an increased resistance since less energy is pushed into the cells per unit time. In other words, the energy supplied by the constant voltage source is dissipated at the inter-connecting resistance rather than charging the cells. This however keeps the cell temperature low thereby reducing the rate of growth of the SEI layer due to temperature. The variation of SEI resistance of the cell with inter-connecting resistance after a hundred charge-discharge cycles is plotted in Fig. 5b. The change in SEI resistance is minimal with increase in inter-connecting resistance, although a slight variation can be seen at higher inter-connecting resistance. The difference in charging current from $Cell_1$ to $Cell_2$ is less than 2 A for the highest inter-connecting resistance.

Fig. 5c shows the variation of SEI layer resistance with different exchange current densities for solvent reduction reaction. The cell is started with initial resistance $\Omega_{SEI} = 500\ \Omega cm^2$ to simulate the conditions when the pack is aged. The solid lines indicate $Cell_1$ resistance whereas the points indicate the $Cell_2$ resistance. The cell-to-cell variation in SEI resistance is "very weak" for both exchange current densities. However a slight difference is visible for cases with high inter-connecting resistances. As shown in Fig. 5a, a high resistance can drive more differential current into the cells resulting in differential capacity fade. Thus it is always advised to operate this pack layout with as low an interconnecting resistance as possible so that the SEI triggered imbalance in the current will be minimised. The observed variation is not powerful enough to cause imbalance or differential ageing in the pack unless other factors supplement the ageing mechanism.

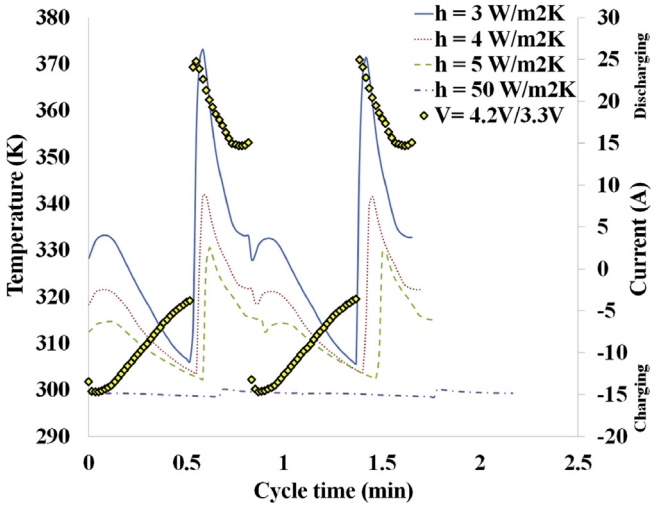

Fig. 6. Temperature variation in the pack with change in heat transfer coefficient (h).

5.4. Thermal effect on the performance of the battery pack

Fig. 6 shows the thermal response of the model by varying the surface heat transfer coefficient at different values for $Cell_1$. The pack is cycled between PCV = 4.2 V and PDV = 3.3 V and the current variation is marked in the figure with hexagonal dots. The ambient temperature is kept at 298.15 K and the convective heat transfer coefficient of the pack is varied from 3 to 50 W/m^2K to control the heat transfer out of the battery. The observation is made for a parallel configuration with zero inter-connecting resistance. The temperature of the battery shows cyclic variation for all heat transfer coefficient values and the cyclic variation reduces with higher heat transfer coefficient as more thermal energy is convected out. The peak temperature in the battery is observed to be 370 K which is well above the safe operating limit of the battery for the 3 W/m^2K condition. Heat transfer of at least 5 W/m^2K is needed to bring the battery temperature down to an operating limit of 330 K. This indicates that the battery cannot be operated under natural convection where the heat transfer coefficient can be much below this limit. The battery can be cooled to a safe limit using any of the forced convection methods such as fan cooling or turbulent aided cooling. Similar observations have been made by Cai and White [5] by varying the cell heat transfer coefficient from adiabatic to iso thermal leading to a peak temperature of 379 K and 298 K respectively. From Fig. 6, the temperature reaches its peak while the rate of change of current is at its maximum. A rapid current change always triggers rapid chemical changes inside the battery followed by a sharp increase in reaction heat Q_{rxn} and ohmic heat Q_{ohm} due to the change in potential gradient. The rapid current variation also results in a rapid rate of change of C-rate almost equal to 4C within

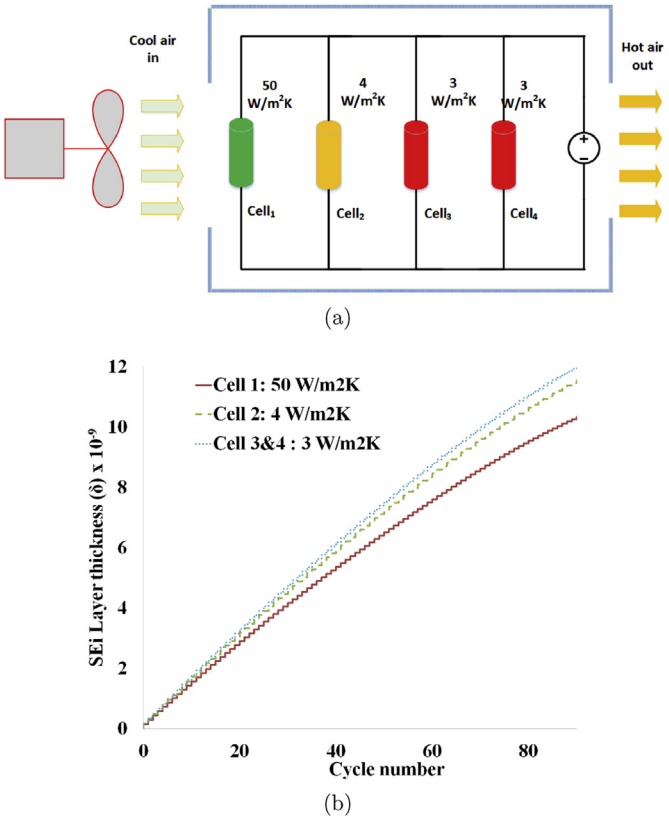

Fig. 7. SEI thickness and the pack layout for a side-cooled configuration (a) Battery pack layout with fan position (b)Charging current with different heat transfer coefficient.

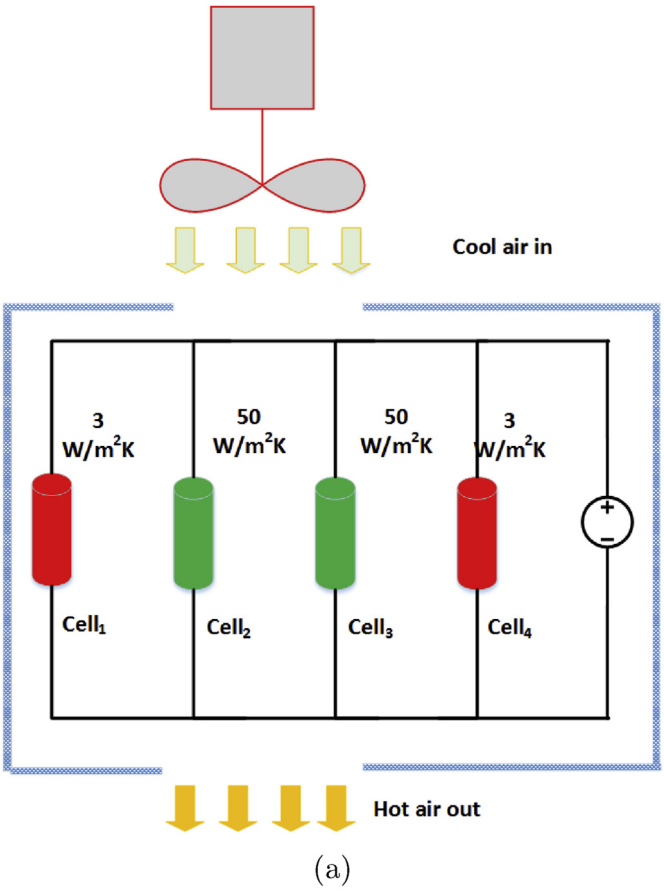

Fig. 8. Split current variation and the battery layout for a top-cooled configuration (a) Battery pack with an outer insulation and its position with respect to air flow (b) Charging current with different heat transfer coefficient and porosity.

a shot duration. A higher C-rate results in an increased temperature and the dependency of C-rate on temperature can be found in Cai and White [5]. We can observe that the temperature is lagging behind the current pulse and the phase lag is dependent on the heat capacity and the thermal conductivity of the cell; the higher the heat capacity, the larger the phase lag. Thus the temperature peaks can be observed at the beginning of charging and the switch over of current from positive to negative. The battery pack reaches 370 K with 3.0 W/m^2K indicating that higher cooling is required for the pack compared to a single cell. More details about the single cell model can be found in Ashwin et al. [21]. The difference in temperature can possibly accelerate the rate of SEI growth in the pack which will be analysed in the coming sections.

Fig. 7 and Fig. 8 shows the effect of temperature on performance of the battery pack in terms of SEI thickness and charging current. The results present a pack with differentially cooled battery and its effect on ageing and charging current variation. The interconnecting resistance is taken as zero so that the current distribution is equal in all cells which gives the flexibility of analysing the effect of thermal effects. In Fig. 7, a practical case is considered where the outer most cell, $Cell_1$, receives the maximum cooling and the innermost cells ($Cell_3$ and $Cell_4$) receives comparatively less cooling. This condition is achieved by imposing a variation in heat transfer coefficient for each cell in the pack. The SEI thickness is plotted for the individual cells with cycle number. We can clearly see a higher SEI growth for cases with lower heat transfer coefficient even for relatively small difference. Thus the impact of thermal imbalance on SEI layer is much more than the imbalance caused by the inter-connecting resistances (R_c)

Fig. 8 shows the split current distribution to the cell branches with different heat transfer coefficient. The heat transfer coefficient for $Cell_2$ and $Cell_3$ is kept higher compared to the outer cells, $Cell_1$ and $Cell_4$. This is equivalent to using a fan or blower which can possibly increase the heat transfer coefficient to a forced convection limit of 50 W/m^2K. The current imbalance is plotted for a constant porosity case and a variable porosity case. There can be initial disturbance or current fluctuation in the pack which will settle down quickly and reach a steady state after few time steps. Lower temperature on $Cell_2$ decelerates the growth of SEI layer thereby decreasing the overall resistance of the cell. However a higher temperature on $Cell_1$ accelerates the SEI growth thereby increasing the overall resistance of the cell causing a lower current flow.

6. Discussion

Fig. 3 shows that the PCV can affect the charging current profile of the pack. The ageing reaction is active only during charging and comparatively insignificant during discharge therefore the ageing side reaction is neglected in this model during discharge. Many of the previous experimental and theoretical investigations show that neglecting the SEI growth during discharge is an acceptable assumption [25,26]. Thus the PCV can affect the life of the battery leading to accelerated ageing in a constant voltage charging configuration. The voltage profile changes after 50 cycles, which shows that a differential SEI build-up can alter the split current distribution in the pack.

From the voltage and current profile analysis, the work proves that cell-to-cell SEI pattern can exist in the pack with different charge-discharge conditions even for identical internal R_c. However there are some additional factors that may be important:

1. In Section 5.1 the investigations were performed with constant temperature. There is also a possibility that the thermal variation can affect the current distribution or the differential porous filling leading to stress development in the pack.
2. Wu et al. [18] proved that the value of inter-connecting resistance is critical in deciding the performance of the battery pack, however this work did not answer whether a change in R_c results in a differential SEI formation possibly leading to accelerated ageing of the pack.

The following sections will attempt to analyse each case in detail to find an answer to the above mentioned questions.

6.1. Discussion on porosity change

The fundamentals of porosity change in a single cell can be seen in Sikha et al. [19] for iso-thermal conditions. Thus the model was not coupled with the energy equation to analyse the effect of thermal heating on porous filling. Fig. 4 shows that the current model is capable of predicting the porosity change pattern in the pack due to the solvent reduction side reaction and analysing the effect of thermal variation on porosity change. There is more intense porous filling for the cells kept at a higher temperature. This can possibly explain the stress development in a differentially cooled pack which can obviously occur in an automotive pack. The internal pressure is proved to have influence on the performance of a battery. A similar observation has been made by Barai et al. [27] for a single cell Lithium-Sulfur battery that non-uniform precipitation may lead to significant pore confinement, which could have the potential to cause microcrack formation in the pore walls of a typical carbon-based cathode microstructure.

6.2. Discussion on capacity fade with R_c

Section 5.3 shows that the pack develops almost uniform cell to cell SEI pattern even with the highest inter-connecting resistance studied $R_c = 1.0 \times 10^{-2}\Omega$. Fig. 5a shows the current distribution to each cell in the pack. The value of the inter-connecting resistance must be carefully adjusted while inter-connecting differentially aged cells which can further widen the imbalance in current flow thereby accelerating the SEI growth. A similar analysis can be seen in Wu et al. [18] to calculate the split current variation. However, the present work takes the analysis further in the ageing context, to study the sensitivity of R_c on a cell-to-cell differential SEI pattern.

The capacity fade for a single cell is almost linear with i_{os} [3,21]. However the capacity fade can be accelerated within a range of exchange current densities and the range is strongly linked to the cell chemistry; more details can be found in Ramadass et al. [3]. Fig. 5c shows that a higher exchange current density i_{os} can accelerate ageing; however very weak cell-to-cell differential ageing can be observed in the pack, even with highest value of split current variation. Hence the split current imbalance due to R_c change may not significantly affect the ageing behaviour of the pack. A similar observation was made by Kenney et al. [13] who used SP model to analyse the capacity fade in a pack with Constant Current(CC) cycling.

The time varying current creates a time varying growth rate for SEI which will be maximum at the beginning of the cycle and then reduces to a lower value, depending on the current profile. The higher the time spent by the pack in high current region during charging, the thicker the SEI growth. The battery analysed in this work quickly allows the current profile to reach an asymptotic lower value within a short time keeping the SEI growth rate lower. The time for charging can also affects the SEI growth. Fig. 3c shows that the cell takes almost 8 h to complete charging. The higher the time spent for charging, the thicker the SEI growth since the side reactions are active especially during charging. The difference in cell current at the beginning of a charging cycle is responsible for the slight difference in SEI growth in the pack. These observations are made for an iso-thermal condition. The effect of temperature increase due to high current and the resulting enhancement in SEI growth rate is completely neglected. Another advantage of using this battery pack layout is that the voltage distribution and the current distribution is not affected by the build-up of SEI layer, or it affects the pack almost uniformly. The battery ages almost equally, developing a similar SEI resistance pattern on the individual cells.

6.3. Discussion on the thermal performance of cells

Section 5.4 and Fig. 6 shows that the pack exhibited a cyclic temperature variation and the maximum temperature was observed at the instances when the rate of change of current is maximum. Hence this model gives insight into the design of the cooling strategy for the battery pack. The phase lag between current signal and the temperature output is proportional to the heat capacity (C_p) of the cell.

The dependency of temperature on SEI growth, capacity fade and power fade is well established [28]. A thermal gradient exists in the battery which affects the performance during charge and discharge. Troxler et al. [29] developed a model to quantify thermal gradient errors due to a lumped parameter approximation. Thus, the model described in this paper uses a discrete thermal model which models the node-to-node heat transfer therefore the model presented can accurately calculate the thermal gradient inside the battery and hence a coupled-differential SEI growth. The accuracy of a thermal model in a pack will be higher if a discrete thermal model is used to calculate cell-to-cell SEI growth. Yang et al. [30] developed a thermal model to investigate the temperature variation external to a battery pack, linked to an electrochemical model. The present model combines the advantage of all the above thermal methods by combining a strong internal as well as external prediction to make a better model for real world applications. Fig. 7 shows that higher temperature can further increase the rate of SEI build-up, and Fig. 8 shows that the thermal imbalance is more critical than the R_c variation, which can develop into a variation in the split current leading to pack current imbalance. Fig. 8 showed an extension of the study presented in Fig. 7 which showed that a variable thermal condition can ultimately lead to a variation in the split current in the pack. The variable porosity also has an effect on the current distribution which reduces the charging current indicating that the variable porosity acts as a resistance on individual cells. It is worth noting that the effect of variable porosity on split current is minimal for up to fifty charge discharge cycles but the difference increases as the cycle number increases. The solvent reduction side reaction at a constant temperature does not alter the current distribution to an individual cell significantly whereas the differentially cooled cells can lead to a large difference in expected lifetime.

Although this work tries to separate the effects on life of the battery into ageing and thermal, the overall impact is always coupled. The pack is not able to operate under natural convection conditions with the configuration presented in Fig. 1.

As a concluding remark, the model presented in this paper can be extended to a pack with cells of any configuration with different initial conditions, capacity and thermal conditions. Moreover this method is capable of analysing the interlinked effects on individual cell performance.

7. Conclusion

A P2D model has been extended to capture the significant electro-chemical effects such as ageing, porosity variation and temperature, inside a battery pack under cyclic charging and discharging conditions. The individual cells in the pack develop uniform SEI resistance indicating that the pack is stable without significant split current variation even for the highest value of inter-connecting resistance studied. This study shows that thermal effects have a higher influence than all other factors considered in this study on the performance of the individual cells indicating the necessity for careful cooling strategy. The porous filling is found to

be more for the cells kept at higher temperatures. A differential thermal condition can accelerate the SEI growth, possibly leading to differential internal stress development and spilt current variation. Thus, this study integrates the capacity fading, thermal heat generation and the porosity change with a variable SEI resistance and the results show that all the coupled electro-chemical and thermal characteristics can be predicted using this pack model.

Acknowledgement

This work was funded by the Innovate UK through the WMG centre High Value Manufacturing (HVM) Catapult in collaboration with Jaguar Land Rover and TATA Motors European Technical Centre. The authors thank Dr. Gael Chouchelamane, Specialist Engineer at Jaguar Land Rover and Dr. Shriram Santhanagopalan, National Renewable Energy Laboratory, US, for helpful discussions.

Nomenclature

a	Active surface area per electrode unit volume (cm^{-1})
A	Electrode plate area (cm^2)
c	Volume-averaged concentration (mol cm^{-3})
C_p	Specific heat (J kg^{-1} K^{-1})
$Cell_n$	Cell number
D	Diffusion coefficient (cm^2 s^{-1})
E	Activation energy (J mol^{-1})
F	Faraday constant, 96487 C mol^{-1}
$f^{\pm}$	Electrolyte activity coefficient
G	Resistance of SEI (Ω cm^2)
h	Convective heat transfer coefficient (W m^2 K^{-1})
I_{app}	Applied current (A)
i_o	Exchange current density for intercalation reaction (A cm^{-2})
i_{os}	Exchange current density for solvent reduction reaction (A cm^{-2})
J_1	Reaction current for intercalation reaction (A cm^{-3})
J_s	Reaction current for solvent reduction reaction (A cm^{-3})
I	Current (A)
k_{ct}	Kinetic rate constant for intercalation reaction
L	Length of electrode (cm)
M_{SEI}	Molecular weight (kg mol^{-1})
Q	Heat generation (W cm^{-3})
R	Universal gas constant, 8.3143 (J mol^{-1} K^{-1})
R	resistance (Ω)
R_c	Inter-connecting resistance (Ω)
t	Time (s)
t_+^0	Transference number
x	Cartesian coordinates
T	Absolute temperature (K)
U, OCV	Open-circuit potential(V)
V	Cell voltage (V)
V_{Li^+}, V_{Lac}	Partial molar volume for intercalation and side reaction (cm^3 mol^{-1})

Greek symbols

α_a, α_c	Charge-transfer coefficient
δ	Thickness (cm)
β	Matrix coefficient
ε	Volume fraction of domain
ρ	Density (kg cm^{-3})
η	Over potential (V)
κ_D	Diffusivity (A cm^{-1})
Λ_s	Radius of particle (cm)
λ	Thermal conductivity (W cm^{-1} K^{-1})
κ_{SEI}	Conductivity of SEI layer (S cm^{-1})
σ	Solid phase conductivity (S cm^{-1})
ϕ	Volume averaged potential (V)
Ω_{SEI}	Initial resistance of SEI layer (Ω cm^2)

Superscript & subscript

amb	Ambient condition
app	Applied voltage or current to the cell or pack
cell	Cell number
e	Electrolyte phase
eff	Effective
film	SEI layer thickness
i	Electrodes
max	Maximum
n	Negative electrode
N	Cycle number
ohm	Ohmic
p	Positive electrode
ref	Reference
react	Reaction
rev	Reversible
s	Solid phase of positive or negative electrode
sur	Surface quantity
$-$	To the left of an interface
$+$	To the right of an interface

List of acronyms

BMS	Battery Management System
CC	Constant Current
CV	Constant Voltage
ECM	Equivalent Circuit Model
EChM	Electrochemical model
LCV	Lower Cut off Voltage of individual cell
OCV	Open Circuit Voltage
P2D	Pseudo Two Dimension
PCV	Pack Charging Voltage
PDV	Pack Discharge Voltage
SEI	Solid Electrolyte Interphase
SoC	State of Charge
SP	Single Particle Model
UCV	Upper Cut off Voltage of individual cell

References

[1] M. Doyle, T.F. Fuller, J. Newman, J. Electrochem. Soc. 140 (1993) 1526–1533.
[2] K. Smith, C.-Y. Wang, J. Power Sources 160 (2006) 662–673.
[3] P. Ramadass, B. Haran, P.M. Gomadam, R. White, B.N. Popov, J. Electrochem. Soc. 151 (2004) A196–A203.
[4] Y. Xie, J. Li, C. Yuan, J. Power Sources 248 (2014) 172–179.
[5] L. Cai, R.E. White, J. Power Sources 196 (2011) 5985–5989.
[6] Y. Ye, Y. Shi, N. Cai, J. Lee, X. He, J. Power Sources 199 (2012) 227–238.
[7] M. Dubarry, N. Vuillaume, B.Y. Liaw, J. Power Sources 186 (2009) 500–507.
[8] J. Kim, J. Shin, C. Chun, B. Cho, Power Electron. IEEE Trans. 27 (2012) 411–424.
[9] C. Sen, N.C. Kar, in: Vehicle Power and Propulsion Conference, IEEE, 2009, pp. 207–212. VPPC'09. IEEE.
[10] R.C. Kroeze, P.T. Krein, in: Power Electronics Specialists Conference, IEEE, 2008, pp. 1336–1342. PESC 2008. IEEE.
[11] K.A. Smith, C.D. Rahn, C.-Y. Wang, J. Dyn. Syst. Meas. Control 130 (2008) 011012.
[12] J.L. Lee, A. Chemistruck, G.L. Plett, J. Power Sources 220 (2012) 430–448.
[13] B. Kenney, K. Darcovich, D.D. MacNeil, I.J. Davidson, J. Power Sources 213 (2012) 391–401.
[14] S. Santhanagopalan, Q. Guo, R.E. White, J. Electrochem. Soc. 154 (2007) A198–A206.
[15] H. Sun, X. Wang, B. Tossan, R. Dixon, J. Power Sources 206 (2012) 349–356.
[16] B. Severino, F. Gana, R. Palma-Behnke, P.A. Estévez, W.R. Calderón-Muñoz, M.E. Orchard, J. Reyes, M. Cortés, J. Power Sources 267 (2014) 288–299.
[17] A. Mills, S. Al-Hallaj, J. Power Sources 141 (2005) 307–315.
[18] B. Wu, V. Yufit, M. Marinescu, G.J. Offer, R.F. Martinez-Botas, N.P. Brandon, J. Power Sources 243 (2013) 544–554.
[19] G. Sikha, P. Ramadass, B. Haran, R.E. White, B.N. Popov, J. power sources 122 (2003) 67–76.

[20] L.H. Saw, Y. Ye, A.A. Tay, W.T. Chong, S.H. Kuan, M.C. Yew, Appl. Energy 177 (2016) 783–792.
[21] T.R. Ashwin, Y.M. Chung, J. Wang, J. Power Sources 328 (2016) 586–598.
[22] G. Sikha, B.N. Popov, R.E. White, J. Electrochem. Soc. 151 (2004) A1104–A1114.
[23] S. Patankar, Numerical Heat Transfer and Fluid Flow, CRC press, 1980.
[24] T.R. Ashwin, G. Narasimham, S. Jacob, Int. J. Heat Mass Transf. 54 (2011) 3357–3368.
[25] S. Santhanagopalan, Q. Guo, P. Ramadass, R.E. White, J. Power Sources 156 (2006) 620–628.
[26] J. Vetter, P. Novák, M. Wagner, C. Veit, K.-C. Möller, J. Besenhard, M. Winter, M. Wohlfahrt-Mehrens, C. Vogler, A. Hammouche, J. power sources 147 (2005) 269–281.
[27] P. Barai, A. Mistry, P.P. Mukherjee, Extreme Mech. Lett. (2016).
[28] M.B. Pinson, M.Z. Bazant, J. Electrochem. Soc. 160 (2013) A243–A250.
[29] Y. Troxler, B. Wu, M. Marinescu, V. Yufit, Y. Patel, A.J. Marquis, N.P. Brandon, G.J. Offer, J. Power Sources 247 (2014) 1018–1025.
[30] N. Yang, X. Zhang, G. Li, D. Hua, Appl. Therm. Eng. 80 (2015) 55–65.